Towards Engineering Chiral Rodlike Metal-Organic Frameworks with Rare Topologies

Thais Grancha,[†] Jesús Ferrando-Soria,*[,†] Davide M. Proserpio,[‡,#] Donatella Armentano*[,§] and Emilio Pardo*[,†]

[†]Departament de Química Inorgànica, Instituto de Ciencia Molecular (ICMOL), Universitat de València, 46980 Paterna, València, Spain

[‡]Dipartimento di Chimica, Università degli Studi di Milano, Via Golgi, 19 - 20133 Milano, Italy

#Samara Center for Theoretical Material Science (SCTMS), Samara State Technical University, Samara 443100, Russia.

[§]Dipartimento di Chimica e Tecnologie Chimiche, Università della Calabria, Rende 87036, Cosenza, Italy

Supporting Information Placeholder

ABSTRACT: The establishment of novel design strategies to target chiral rodlike MOFs, elusively faced until now, is one of the most straightforward manners to widen the scope of MOFs. Here we describe our last advances on the application of the metalloligand design strategy towards the development of efficient routes to obtain chiral rodlike MOFs. To this end, we have used as precursor an enantiopure homochiral hexanuclear wheel (**1**), derived from the amino acid *D*-valine, which after a supramolecular reorganization into a one-dimensional homochiral chain – with the same configuration as **1** – lead to the formation of an homochiral rodlike MOF (**2**) exhibiting rare **etd** topology.

Metal-organic frameworks (MOFs)[1-5] are a class of porous crystalline materials, with fascinating architectures and a myriad of interesting physical and chemical properties,[6-10] which have situated them in an advantageous position among other materials. This exponential growth has been underpinned, to some extent, on the thorough quest of rational design strategies to build/functionalize – in a controlled manner – MOFs with predetermined dimensionalities and topologies,[11-13] and the possibility to use X-ray crystallography to follow and rationalize the proposed synthetic methodology.[14-16] These have enable MOFs to find applications in such diverse fields as gas adsorption and separation,[17-20] catalysis,[21,22] molecular recognition processes,[23,24] drug delivery,[25,26] magnetism[27,28] and water remediation.[29-31]

However, this has not been the case for MOFs constructed from one-dimensional (1D) rod-like Secondary Building Units (SBUs).[32] Despite the thrilling physical properties exhibited by rod MOFs,[18,33-35] the efforts to implement efficient design strategies to target them have been scarce, and the most common method has been based on trial and error assays. At the same time, the number of chiral MOFs[36,37] is quite limited when compared to non-chiral ones, which is intimately connected to the synthetic difficulties and the resultant necessity to improve the current used approaches.[38-41] This lacuna becomes even more significant when dealing with chiral rod-based MOFs, where the investigations are in its infancy.[32,42-44] At this respect, the only two remarkable advances have been based on the use of a heterotritopic ligand, with preference to form helical rods,[43] and the use by our group of preformed chiral chains as building blocks.[44]

In this work, aiming at shedding some more light on the required self-assembly conditions leading to chiral rod-like MOFs, we have continued our investigations on the potential of the metalloligand[45] design strategy with oxamato-based ligands derived from natural amino acids.[16,22,37,41,46] Thus, we have further explored this strategy based on the use of enantiopure ligands able to efficiently transmit, in a first stage, the encoded chiral information to an homochiral wheel. Then, in a second stage, it takes place a supramolecular reorganization leading to homochiral 1D rodlike building blocks, which exhibits free carbonyl groups able to further coordinate to square planar metal complexes,[47] yielding a three-dimensional (3D) chiral rodlike MOF.[44] Despite in this case the chiral 1D polymeric SBU is not isolated, the cornerstone of the design strategy – to efficiently transfer the chiral information from the ligands to the MOF through a molecular-based preformed building block – is maintained. This new finding broadens the range of precursors able to assembly, in a controlled manner, chiral rod MOFs and represents another evidence of the potential of supramolecular adaptive chemistry.[48]

Here, we report the use of a previously reported enantiopure hexanuclear copper(II) wheel – prepared using an oxamato-based ligand derived from the amino acid *D*-valine[49] – with formulae $(Me_4N)_6\{Cu^{II}_6[(R)\text{-valma}]_6\} \cdot 7H_2O$ (**1**) [where (*R*)-valma = (*R*)-*N*-(ethyl oxoacetate)valine] (Figure 1 and Scheme S1, Supporting Information) as a chiral preformed metalloligand.

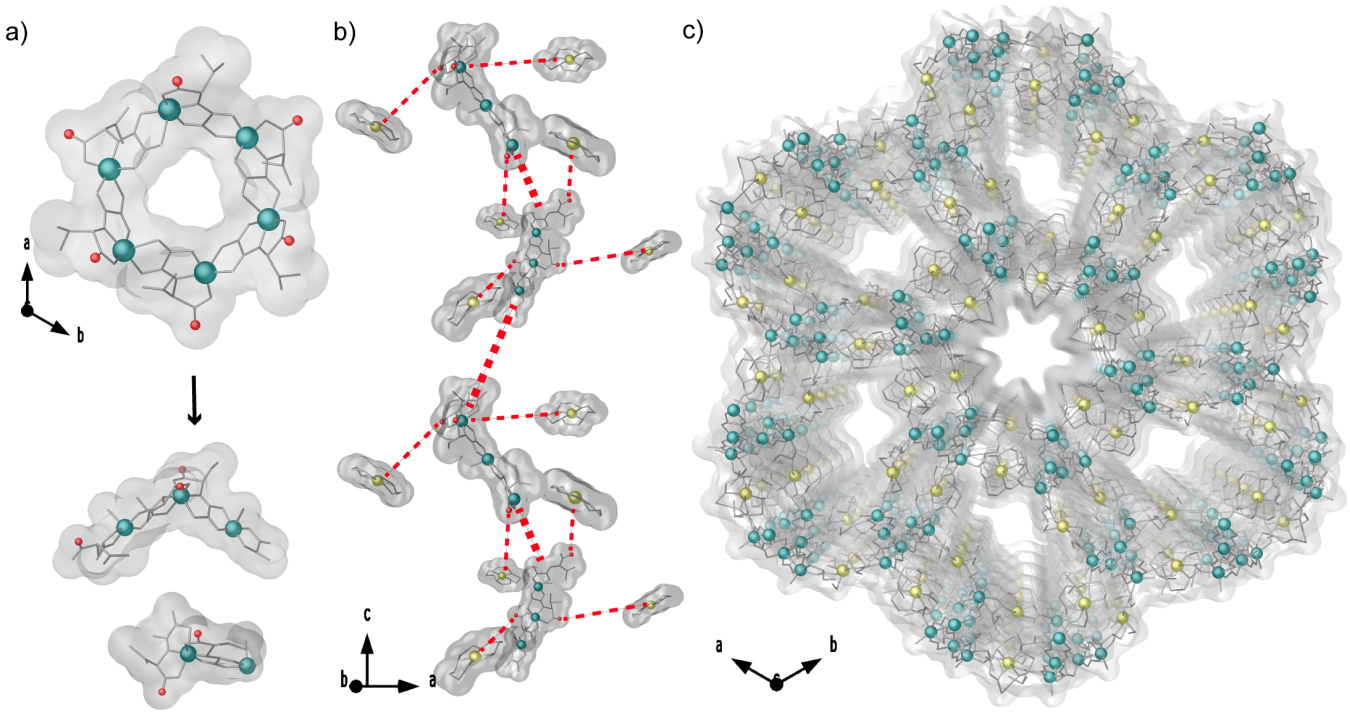

Figure 1. (a-c) Chemical "metalloligand" approach: Perspective views of the precursor compound **1**[49] (top a) and of **2** (c). Supramolecular reorganization from an enantiopure homochiral hexanuclear copper(II) wheel into a homochiral 1D rodlike building block and suggested self-assembling process consisting of the coordination of the free carbonyl groups of **1** towards $[Ni(cyclam)]^{2+}$ cations (b). Perspective view of the 3D homochiral MOF **2** (c). The copper(II) and nickel(II) ions and the free carbonyl groups are represented by cyan, gold and red spheres, respectively, whereas the ligands are depicted by sticks. Thin and thick dotted lines simulate the approach of $[Ni(cyclam)]^{2+}$ cations to the free carbonyl groups and the self-assembly of oligomers (bottom a) forming the chain, respectively.

After reacting the hexacopper(II) units, with free carbonyl groups, towards square planar mononuclear cations $[Ni(cyclam)]^{2+}$ (Figures 1-4 and S1-S8, Supporting Information), a new homochiral 3D MOF of formula $[Ni(cyclam)][Cu^{II}(R)\text{-valma}]_2 \cdot 15H_2O$ (**2**) with rare **etd** topology was obtained (Figures S8-S10).

The chemical identity of **2** was established by the combination of ICP-AES, EDX, elemental, PXRD and TGA analyses (Figures S11-S13 Supporting Information). In addition, the crystal structure of **2** could be determined by single crystal X-ray diffraction (see Experimental Section, Supporting Information)

Crystal Structure. **2** crystallizes in the hexagonal chiral space group $P6_5$. Overall, 3D framework of **2** is built by chiral left-handed copper(II) parallel chains, interconnected by $[Ni(cyclam)]^{2+}$ ions (Figure 1c and Figures S1-S7), to give a nanosized tubule with an opening size of 1.2 nm – measured from van der Waals surfaces – along the *c* axis (Figure S4). Each tubule/channel shares metal-carboxylate chains – grasped by $[Ni(cyclam)]^{2+}$ complexes acting as ditopic *metallolinkers* – with neighboring ones, leading to a chiral porous three-dimensional framework (Figure 1c and Figures S3-S5). PLATON analysis revealed that the three-dimensional structure is composed of large solvent-accessible voids of 29348.8 A^3 which constitute 65% of volume per unit cell [44954.0 (**2**)].

Eight Cu^{2+}, eight L [(*R*)-$valma^{3-}$] ligands, and four $[Ni(cyclam)]^{2+}$ ions are present in the asymmetric unit of **2** (Figure S1). All Ni^{2+} metal ions are axially coordinated by two oxygen atoms of two free carbonyl groups from consecutive valine amino acid residues [Ni-O bond lengths ranging from 2.04(1) to 2.23(2) Å], whereas four nitrogen atoms of the cyclam ligand define the equatorial plane [Ni-N distances ranging from 1.90(2) to 2.34(1) Å] of a distorted octahedral geometry (Figure S1). For the sake of clarity, copper(II) metal cations can be divided in two groups depending on their local environment. Four of them – Cu(2), Cu(3), Cu(6) and Cu(8) – exhibit a highly distorted octahedral environment (CuN_2O_4), being coordinated to two tridentate valine residues of (*R*)-$valma^{3-}$ ligand. Conversely, Cu(1), Cu(4), Cu(5) and Cu(7) are coordinated only by oxygen atoms from both the carboxylate groups of two $valma^{3-}$ ligands and terminal water molecules (Figure 2).

Overall, not equivalent Cu^{2+} alternate in two independent helical chains with *M* handedness of the type $[Cu_2(L)_2]n$ growing along the *c* axis, and are sequentially linked by two bridging/bidentate carboxylate groups and two bridging/tridentate oxalamino (Figures 2e-4 and Figures S1 and S5c). As shown in Figure 4, the $[Cu^{II}(R)\text{-valma}]^{2-}$ chains, constituting the 1D-SBUs, are connected by $[Ni(cyclam)]^{2+}$ complexes acting as ditopic *metallolinkers*.

MOFs build by rod-like SBUs are usually described by looking at the packing of the rods and how they are linked.[32,42,50] It is common to find structures built by parallel rods to exhibit axes on symmetric square (**sql**), honeycomb (**hcb**) or Kagomé (**kgm**) nets.[51] Looking at **2** down the c axis the rods describe an **hcb** pattern but with some remarkable features. The two crystallographically different $[Cu_2(L)_2]_n$ polymers, growing along *c* axis (Figures 4-5a), intersect the *ab* plane forming four crystallographically distinct chiral

channels (Figure 5) of different size and shape. Two large hexagonal channels aligned parallel to the *c* axis (Figures S6 and S7), with accessible diameters of *ca.* 1 and 0.8 nm, one of them being more regular (Figure 5b, pore A, including equivalent chains) respect to a second one highly distorted (Figure 5b, pore B, comprising crystallographically distinct chains), and two rectangular (C and D in Figure 5b) very small channels with a narrow window of approximatively 5 x 4 Å – not so accessible considering the van der Waals radii of carbon and nitrogen atoms of the cyclam ligand of the pore's walls filling the space.

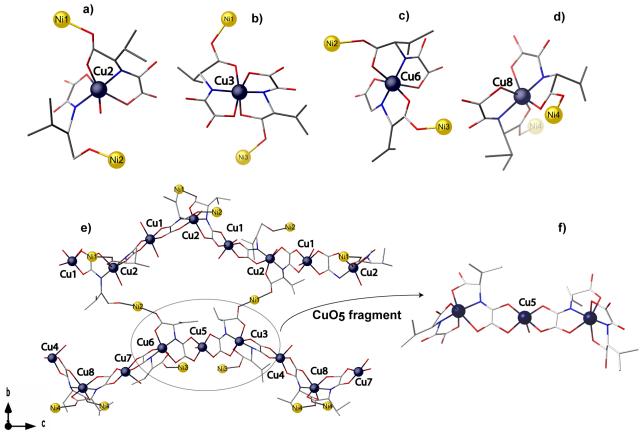

Figure 2. Details of copper environments in **2**. (Copper: dark blue; Nickel: gold; Carbon: grey; Nitrogen: blue and Oxygen: red).

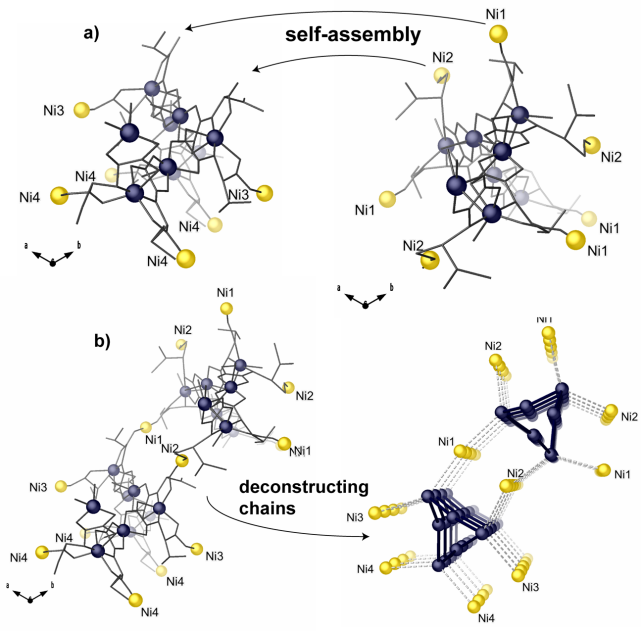

Figure 3. Suggested self-assembly in **2** of *M* helical chains and $[Ni(cyclam)]^{2+}$ complexes. Colors are as in Figure 2.

The hexagonal channels are not interlocked to any of the other channels and are delimited by a double wall of $[Ni(cyclam)]^{2+}$ complexes acting as ditopic *metallolinkers*. In fact, the structure of **2** can be seen as a really fashionable packing of diverse helical chains generated by the coordination of $[Ni(cyclam)]^{2+}$ with valma amino acid residues (Figure 6 and Figures S6-S7). Bearing in mind the description of channels and their double walls, it is possible to define four helices generating inner and outer walls of the two hexagonal channels (Figure 6, see also Figures S6-S7), where the double link of $[Ni(cyclam)]^{2+}$ units is most likely at its origin.

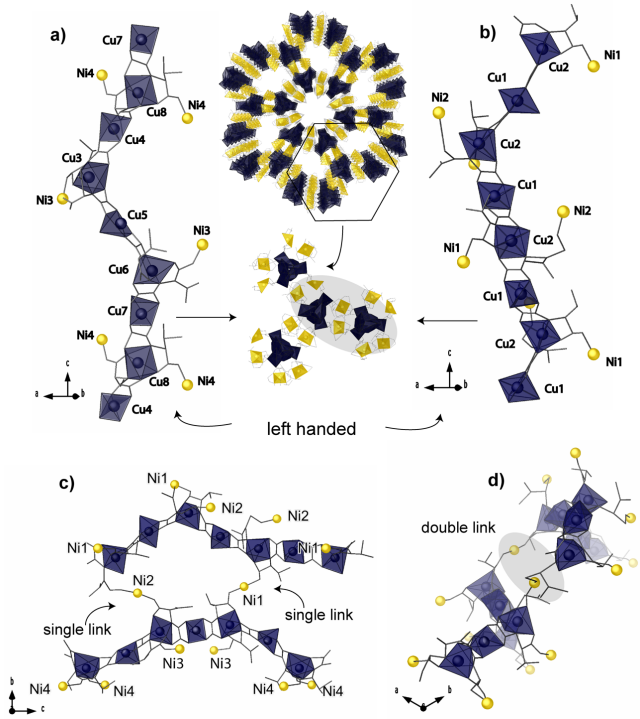

Figure 4. Perspective views of a fragment of the two crystallographic distinct chains in **2** (a and b). Views along [011] and [110] directions of the two assembled chains (c and d). Copper–oxygen/nitrogen polyhedral are colored in blue whereas Ni^{2+} cations are represented as gold spheres.

Those double walls are stabilized by C-H···H-C interactions between neighboring cyclam ligands with C···C distances in the range 3.5-4.3 Å (Figure S2).

Further insights of the structure of **2** can be gained by an in depth topological analysis with ToposPro[52] following the guidelines recently outlined by a IUPAC task group.[53] The 3D underlying network is obtained with the "standard simplification" method that associate a node to both metals and ligands. In our case, the Ni and Cu are 2-coordinated nodes, while the ligands are 3-c (linking two copper and one nickel). Thus, it reduces the rod packing MOF to the rare uninodal chiral 3-c **etd** (Figure 5c and Figure S8),[51] very distorted when compared to the ideal **etd** (Figure S9). As far as we know only three chiral MOFs, showing an **etd** underlying net have been reported so far in the ToposPro Toris database.[54] But, what is the relation between this rare net and the **hcb** rod packing observed in **2**? **etd** could be described from three different packing **hcb**, **hxl** and **kgm** as shown in Figure S10. The choice of the description depends on the shape and position of the infinite rod-like SBU. The program ToposPro extract unambiguously the infinite Cu···Cu SBU, using the procedure called "the cluster representation",[53,55] assigning the **hcb** rod-packing.

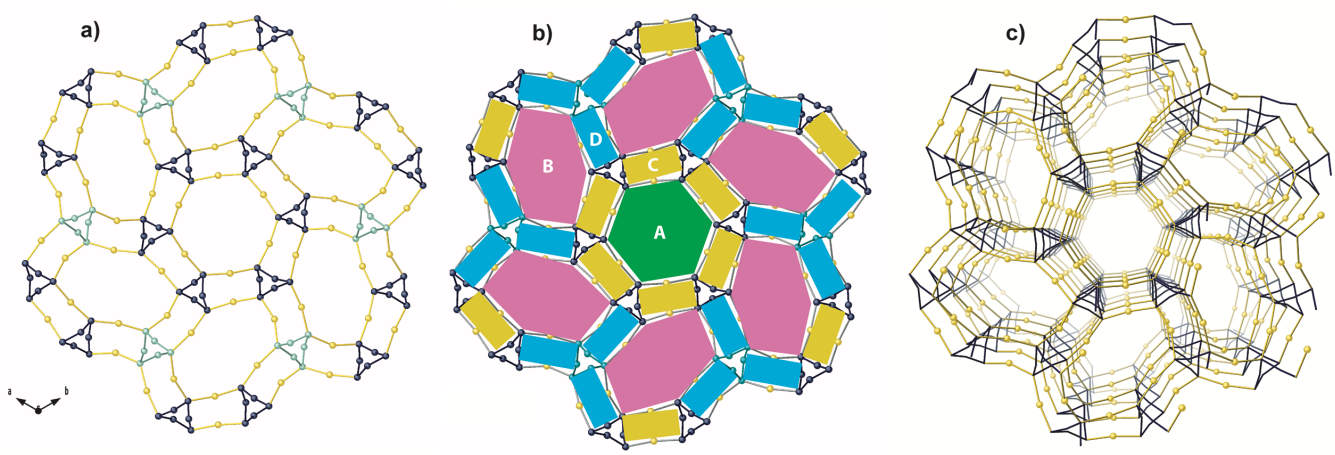

Figure 5. (a-c) Views of the packing of chains in the 2-periodic net. Different colors in b) underline the four different types of polygons/channels in **2** (a and b). Blue and green spheres represent copper metal ions in crystallographically distinct deconstructed chains. c) Perspective view of the 3D underlying 3-coordinated **etd** net, where chiral chains (blue lines) – all with same handedness *M* – are brought together by $[Ni(cyclam)]^{2+}$ complexes (gold spheres) acting as ditopic *metallolinkers*.

Recently we have reported the use of a preformed chiral 1D polymeric SBU for the construction of a new chiral rod-based 3D MOF, exploiting the ability of the oxamato-based derivative of the amino acid *D*-phenylglycine, when reacting the preformed chains towards the square planar mononuclear cation $[Ni(cyclam)]^{2+}$.[44] Despite both valma^{3-} and pegma^{3-} ligands – where (*R*)-pegma = (*R*)-*N*-(ethyl oxoacetate)phenylglycine – exhibit the same exo-hexadentate coordination fashion, the unusual coordination of valma^{3-} ligand leading to the alternation of $CuNO_4$ and CuO_6 entities makes the overall net in **2** very different and extraordinarily intricate respect to previously reported by us with pegma. Indeed in this latter one MOF, helices are all right-handed and linked by $[Ni(cyclam)]^{2+}$ cationic complexes to generate an **eta** net.

In order to have better insights both in structure assembly and in reasons of diversity of **2** respect to pegma one,[44] we analyzed in detail the importance that may play weak C-H···H-C interactions between neighboring valine isopropyl residues and also cyclam ligands on the self-assembling process (Figure S2). Despite the weakness of C-H···H-C interactions,[56] when many are present, they can play a stabilizing role in a range of materials, *e*.g. in lipid membranes,[57] based on their cumulative effect. On this basis, we infer that such C-H···H-C interactions impose the *syn* conformation of valine isopropyl residues (C···C distances of 3.5-4.3 Å, Figure S2) and drive to the unusual coordination of valma ligands (Figure 3), which, in turn, is responsible of the alternation of copper metal ions with different environments (Figures 2 and 4) and, ultimately, dictates the nature of the self-assembled entity (Figures 1c and 5). In fact, as $[(CH_3)_4N]^+$ cations play a crucial role in templating wheel precursors for valma – again according to effectiveness of alkyl-alkyl interactions – and chain SBUs for pegma,[44] it is not hard to believe that also ultimate self-assembly of chiral rod-based MOFs could be driven by 'supramolecular rules' supported on C-H···H-C interactions, in a reminiscent way of the complex functional architectures observed in living beings based in weak supramolecular interactions.[57] Thus, the observed self-organization and adaptive chemistry[48] to obtain **2** represent another level of complexity on the self-assembly of intricate structures and another elegant example towards the emergence of evolutive chemistry.

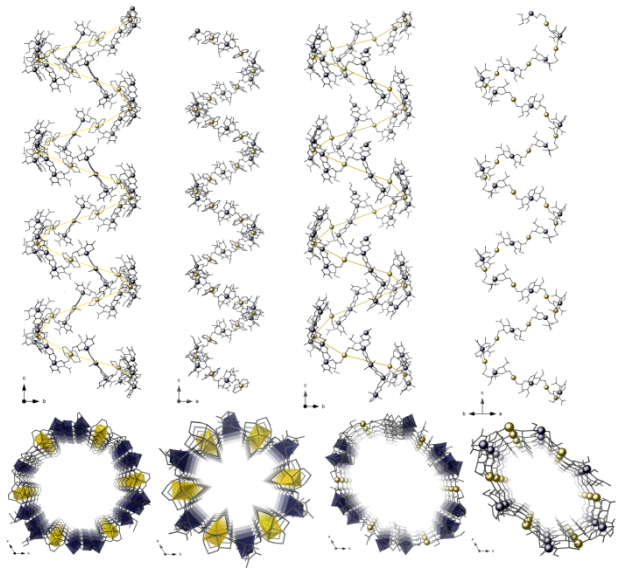

Figure 6. Side and top view of the two chiral hexagonal channels constructed by four helices generating inner and outer walls as a consequence of a double link of $Ni(cyclam)]^{2+}$ units. (See also Figures S6-S7 in Supporting Information)

Thermogravimetric Analysis and X-Ray Powder Diffraction. A consistent powder X-ray diffractogram of the bulk sample with the theoretical one extracted from the crystal selected to single-crystal X-ray diffraction evidence the purity of the bulk sample (Figure S11). Thermogravimetric analysis (TGA) under a dry N_2 flow was used to confirm

the solvent content of **2** (Figure S12 in the Supporting Information).

Circular Dichroism, Electronic Absorption and Diffuse Reflectance Spectroscopy and Mass Spectrometry. Solid circular dichroism (CD) spectrum of **2** was carried out in order to further confirm its enantiomeric nature and it is collected in Figure S13. It exhibits maximum positive Cotton effects at 344 nm, whereas maximum negative effects are observed at 312, 390 and 619 nm. The band in the visible region is attributed to a copper(II) d–d transition, which arises from a chirality induced effect on the copper centers by the enantiopure ligands and it is very similar to that observed in the enantiopure precursor wheels[49] (inset of Figure S13). In turn, those bands observed in the UV region can be assigned to metal-to-ligand (ML) charge-transfer transitions. The electronic spectrum of **1** shows one intense band in the high-energy UV region, together with a Vis band of lower intensity, which correspond to the typical d-d transition of a copper(II) complex. The diffuse reflectance spectrum of **2** shows one intense band in the low-energy UV-region, together with a quite intense Vis band, slightly red shifted respect **1**.

In order to achieve a better understanding of the stable oligomeric species in solution and supramolecular reorganization of **1** into a 1D chiral chains were carried out ESI-MS experiments. H_2O/CH_3CN solutions of **1** and **1** plus $[Ni(cyclam)]Cl_2$ suggest a higher stability of the hexanuclear wheels (inferred by the most intense peak at *m/z* 1531.9, Figure S14) and its reorganization into oligomeric species – trimeric $[H^+{\cdot}Cu_3L_3(TMA)_3]$ and dimeric species $[Cu_2L_2(TMA)_3^+]$ for peaks at *m/z* 970 and 720 (Figures S15-S16, when $[Ni(cyclam)]^{2+}$ complexes are present, which may be consider as precursors of the 1D chiral chains.

Conclusions

We report a novel highly intricate porous chiral bimetallic rod-MOF (**2**), which has been synthesized by using a rational programmed "complex as ligand" approach. Thus – in the presence of cationic mononuclear square-planar complexes with free axial positions such as $[Ni(cyclam)]^{2+}$– anionic enantiopure hexacopper(II) wheels acting as metalloligands disassemble in solution to form enantiopure copper(II) 1D polymers capable to further coordinate the $[Ni(cyclam)]^{2+}$ units to yield the homochiral 3D MOF, where the encoded chiral information of the starting ligands is efficiently transmitted to the final MOF. Indeed, the crystal structure of **2** shows that the MOF is built of helical chains that are connected by $[Ni(cyclam)]^{2+}$ complexes acting as ditopic *metallolinkers*. The result is a fascinating crystal structure with rare 3-coordinated **etd** net. Overall, the crystal structure exhibits four crystallographically independent channels comprising inner and outer walls as result of the binding mode of ditopic metallolinker employed towards rods. A detailed comparison of chains packing in **2** respect to an analogue MOF constructed with similar strategy, previously reported by us, reveals how subtle modifications of the employed ligand can dictate self-assembly finely tuned by apparently weakly but highly efficient supramolecular interactions. Current efforts in our group are devoted to further explored this new adaptive chemistry towards the self-assembly of chiral rod-based MOFs.

EXPERIMENTAL SECTION

Preparation of $[Ni(cyclam)][Cu^{II}(R)\text{-valma}]_2 \cdot 15H_2O$ (2). A multigram scale synthesis of **2** was carried out by direct reaction of 1/9 water/methanol solutions (v/v) of compound **1** and $[Ni(cyclam)]Cl_2$: a 5 mL portion of the $[Ni(cyclam)]Cl_2$ solution (0.83 g, 0.5 mmol) was added dropwise over 10 mL of another solution containing compound **1** (2.07 g, 1 mmol). The mixture was stirred at r.t. for 48 h. The resulting pale green polycrystalline powder was filtered off, gently washed with 1/9 water:methanol (v/v) and air-dried. Yield: 0.36 g, 70 %; Anal.: calcd for $C_{24}H_{70}Cu_2NiN_6O_{25}$ (1028.65): C, 28.02; H, 6.86; N, 8.17%. Found: C, 28.11; H, 6.82; N, 8.19%; IR (KBr): ν = 1639 and 1595 cm^{-1} (C=O).

X-ray quality cubic prisms of **2** were obtained by slow diffusion in an H-shaped tube of 1/9 water:methanol (v/v) containing stoichiometric amounts of **1** in one arm and $[Ni(cyclam)]Cl_2$ in the other one. The crystals were collected by filtration and air-dried.

Single-Crystal X-ray Diffraction. Crystal data for **2**: $C_{96}Cu_8Ni_4H_{280}N_{24}O_{100}$, hexagonal, space group $P6_5$, a = 44.286(3) Å, c = 26.467(2) Å, V = 44954(6) $Å^3$, T = 100(2) K, Z = 6, ρ_{calc} = 0.912 $g.cm^{-3}$, μ = 0.864 mm^{-1}, of the 316825 reflections collected, 50725 are unique and 17518 observed with $I > 2\sigma(I)$. Refinement of 331 parameters gave R = 0.1254 and R_w = 0.2744 for reflections with $I > 2\sigma(I)$ with S = 1.631. CCDC 1849587.

X-ray Powder Diffraction. Polycrystalline sample of **2** was introduced into 0.5 mm borosilicate capillary prior to being mounted and aligned on a Empyrean PANalytical powder diffractometer, using Cu Kα radiation (λ = 1.54056 Å). Five repeated measurements were collected at room temperature (2θ = 2–60°) and merged in a single diffractogram.

Thermogravimetric analysis. The TGA measurement was performed on a crystalline sample of **2** under a dry N_2 atmosphere with a Mettler Toledo TGA/STDA 851^e thermobalance operating at a heating rate of 10 ºC min^{-1}.

ASSOCIATED CONTENT

Supporting Information

Additional preparations and physical characterization data (Circular Dichroism and Mass Spectrometry). Additional Figures (Figures S1-S16) and scheme of ligand. Crystallographic refinement for **2** (Table S1). CCDC 1849587. This material is available free of charge via the Internet at http://pubs.acs.org.

AUTHOR INFORMATION

Corresponding Author

To whom correspondence should be addressed: jesus.ferrando@uv.es; donatella.armentano@unical.it; emilio.pardo@uv.es.

Notes

The authors declare no competing financial interests.

ACKNOWLEDGMENT

This work was supported by the MINECO (Spain) (Project CTQ2016-75671-P and Excellence Unit "Maria de Maeztu" MDM-2015-0538) and the Ministero dell'Istruzione,

dell'Università e della Ricerca (Italy). Thanks are also extended to the Ramón y Cajal Program (E. P.), the "Fondo per il finanziamento delle attività base di ricerca" (D.A.) and the "Subprograma atracció de talent-contractes postdoctorals de la Universitat de Valencia" (J. F.-S.).

REFERENCES

(1) Furukawa, H.; Cordova, K. E.; O'Keeffe, M.; Yaghi, O. M. The chemistry and applications of metal-organic frameworks. *Science* **2013**, *341*, 974.

(2) Eddaoudi, M.; Sava, D. F.; Eubank, J. F.; Adil, K.; Guillerm, V. Zeolite-like metal-organic frameworks (ZMOFs): design, synthesis and properties. *Chem. Soc. Rev.* **2015**, *44*, 228–249.

(3) Cui, Y.; Li, B.; He, H.; Zhou, W.; Chen, B.; Qian, G. Metal-Organic Frameworks as Platforms for Functional Materials. *Acc. Chem. Res.* **2016**, *49*, 483–493.

(4) Islamoglu, T.; Goswami, S.; Li, Z.; Howarth, A. J.; Farha, O. K.; Hupp, J. T. Postsynthetic Tuning of Metal-Organic Frameworks for Targeted Applications. *Acc. Chem. Res.* **2017**, *50*, 805–813.

(5) Maurin, G.; Serre, C.; Cooper, A.; Férey, G. The new age of MOFs and of their porous-related solids. *Chem. Soc. Rev.* **2017**, *46*, 3104–3107.

(6) Inge, A. K.; Köppen, M.; Su, J.; Feyand, M.; Xu, H.; Zou, X.; O'Keeffe, M.; Stock, N. Unprecedented Topological Complexity in a Metal-Organic Framework Constructed from Simple Building Units. *J. Am. Chem. Soc.* **2016**, *138*, 1970–1976.

(7) Li, P.; Vermeulen, N. A.; Malliakas, C. D.; Gómez-Gualdrón, D. A.; Howarth, A. J.; Mehdi, B. L.; Dohnalkova, A.; Browning, N. D.; O'Keeffe, M.; Farha, O. K. Bottom-up construction of a superstructure in a porous uranium-organic crystal. *Science* **2017**, *356*, 624–627.

(8) Kim, H.; Yang, S.; Rao, S. R.; Narayanan, S.; Kapustin, E. A.; Furukawa, H.; Umans, A. S.; Yaghi, O. M. Water harvesting from air with metal-organic frameworks powered by natural sunlight. *Science* **2017**, *356*, 430–434.

(9) Reed, D. A.; Keitz, B. K.; Oktawiec, J.; Mason, J. A.; Runčevski, T.; Xiao, D. J.; Darago, L. E.; Crocellà, V.; Bordiga, S.; Long, J. R. A spin transition mechanism for cooperative adsorption in metal-organic frameworks. *Nature* **2017**, *550*, 96–100.

(10) Shen, K.; Zhang, L.; Chen, X.; Liu, L.; Zhang, D.; Han, Y.; Chen, J.; Long, J.; Luque, R.; Li, Y.; Chen, B. Ordered macro-microporous metal-organic framework single crystals. *Science* **2018**, *359*, 206–210.

(11) Li, M.; O'Keeffe, M.; Yaghi, O. M. Topological Analysis of Metal-Organic Frameworks with Polytopic Linkers and/or Multiple Building Units and the Minimal Transitivity Principle. *Chem Rev.* **2014**, *114*, 1343–1370.

(12) Guillerm, V.; Kim, D.; Eubank, J. F.; Luebke, R.; Liu, X.; Adil, K.; Lah, M. S.; Eddaoudi, M. A supermolecular building approach for the design and construction of metal-organic frameworks. *Chem. Soc. Rev.* **2014**, *43*, 6141–6172.

(13) Cohen, S. M. The Postsynthetic Renaissance in Porous Solids. *J. Am. Chem. Soc.* **2017**, *139*, 2855–2863.

(14) Inokuma, Y.; Yoshioka, S.; Ariyoshi, J.; Arai, T.; Hitora, Y.; Takada, K.; Matsunaga, S.; Rissanen, K.; Fujita, M. X-ray analysis on the nanogram to microgram scale using porous complexes. *Nature* **2013**, *495*, 461–466.

(15) Bloch, W. M.; Champness, N. R.; Doonan, C. J. X-ray Crystallography in Open-Framework Materials. *Angew. Chem., Int. Ed.* **2015**, *54*, 12860–12867.

(16) Mon, M.; Bruno, R.; Ferrando-Soria, J.; Bartella, L.; Di Donna, L.; Talia, M.; Lappano, R.; Maggiolini, M.; Armentano, D.; Pardo, E. Crystallographic snapshots of host-guest interactions in drugs@metal-organic frameworks: towards mimicking molecular recognition processes. *Mater. Horizons* **2018**, *5*, 683–690.

(17) Nugent, P.; Belmabkhout, Y.; Burd, S. D.; Cairns, A. J.; Luebke, R.; Forrest, K.; Pham, T.; Ma, S.; Space, B.; Wojtas, L.; Eddaoudi, M.; Zaworotko, M. J. Porous materials with optimal adsorption thermodynamics and kinetics for CO_2 separation. *Nature* **2013**, *495*, 80–84.

(18) Mason, J. A.; Oktawiec, J.; Taylor, M. K.; Hudson, M. R.; Rodriguez, J.; Bachman, J. E.; Gonzalez, M. I.; Cervellino, A.; Guagliardi, A.; Brown, C. M.; Llewellyn, P. L.; Masciocchi, N.; Long, J. R. Methane storage in flexible metal-organic frameworks with intrinsic thermal management. *Nature* **2015**, *527*, 357–361.

(19) Cadiau, A.; Adil, K.; Bhatt, P. H.; Belmabkhout, Y.; Eddaoudi, M. A metal-organic framework-based splitter for separating propylene from propane. *Science* **2016**, *353*, 137–140.

(20) Li, H.; Wang, K.; Sun, Y.; Lollar, C.; Li, J.; Zhou, H.-C. Recent advances in gas storage and separation using metal-organic frameworks. *Mater. Today* **2018**, *21*, 108–121.

(21) Zhang, X.; Huang, Z.; Ferrandon, M.; Yang, D.; Robison, L.; Li, P.; C Wang, T. C.; Delferro, M.; Farha, O. K. Catalytic Chemoselective Functionalization of Methane in a Metal-Organic Framework. *Nat. Catal.*, **2018**, *1*, 356–362.

(22) Mon, M.; Rivero-Crespo, M. A.; Ferrando-Soria, J.; Vidal-Moya, A.; Boronat, M.; Leyva-Pérez, A.; Corma, A.; Hernandez-Garrido, J. C.; López-Haro, M.; Calvino, J. J.; Ragazzon, G.; Credi, A.; Armentano, D.; Pardo, E. Synthesis of Densely Packaged, Ultrasmall Pt^{0}_{2} Clusters within a Thioether-Functionalized MOF: Catalytic Activity in Industrial Reactions at Low Temperature. *Angew. Chem., Int. Ed.* **2018**, *57*, 6186–6191.

(23) Peng, Y.; Gong, T.; Zhang, K.; Lin, X.; Liu, Y.; Jiang, J.; Cui, Y. Engineering chiral porous metal-organic frameworks for enantioselective adsorption and separation. *Nat. Commun.* **2014**, *5*, 1–9.

(24) Navarro-Sánchez, J.; Argente-García, A. I.; Moliner-Martínez, Y.; Roca-Sanjuán, D.; Antypov, D.; Campíns-Falcó, P.; Rosseinsky, M. J.; Martí-Gastaldo, C. Peptide Metal-Organic Frameworks for Enantioselective Separation of Chiral Drugs. *J. Am. Chem. Soc.* **2017**, *139*, 4294–4297.

(25) Simon-Yarza, T.; Giménez-Marqués, M.; Mrimi, R.; Mielcarek, A.; Gref, R.; Horcajda, P. Serre, C.; Couvreur, P. A Smart Metal-Organic Framework Nanomaterial for Lung Targeting. *Angew. Chem. Int. Ed.* **2017**, *56*, 15565–15569.

(26) Dong, Z.; Sun, Y.; Chu, J.; Zhang, X.; Deng, H. Multivariate Metal-Organic Frameworks for Dialing-in the Binding and Programming the Release of Drug Molecules. *J. Am. Chem. Soc.* **2017**, *139*, 14209–14216.

(27) Darago, L. E.; Aubrey, M. L.; Yu, C. J.; Gonzalez, M. I.; Long, J. R. Electronic Conductivity, Ferrimagnetic Ordering, and Reductive Insertion Mediated by Organic Mixed-Valence in a Ferric Semiquinoid Metal-Organic Framework. *J. Am. Chem. Soc.* **2015**, *137*, 15703–15711.

(28) Li, W.; Sun, L.; Jarillo-Herrero, P.; Dincă, M.; Li, J. High temperature ferromagnetism in π-conjugated two-dimensional metal-organic frameworks. *Chem. Sci.* **2017**, *8*, 2859–2867.

(29) Dias, E. M.; Petit, C. Towards the use of metal-organic frameworks for water reuse: a review of the recent advances in the field of organic pollutants removal and degradation and the next steps in the field. *J. Mater. Chem. A* **2015**, 3, 22484–22506.

(30) Kobielska, P. A.; Howarth, A. J.; Farha, O. K.; Nayak, S. Metal-organic frameworks for heavy metal removal from water. *Coord. Chem. Rev.* **2018**, *358*, 92–107.

(31) Mon, M.; Bruno, R.; Ferrando-Soria, J.; Armentano, D.; Pardo, E. Metal-organic framework technologies for water remediation: towards a sustainable ecosystem. *J. Mater. Chem. A* **2018**, 6, 4912–4947.

(32) Schoedel, A.; Li, M.; Li, D.; O'Keeffe, M.; Yaghi, O. M. Structures of Metal-Organic Frameworks with Rod Secondary Building Units. *Chem. Rev.* **2016**, *116*, 12466–12535.

(33) Bourrelly, S.; Llewelyn, P. L.; Serre, C.; Millange, F.; Loiseau, T.; Férey, G. Different Adsorption Behaviors of Methane and Carbon Dioxide in the Isotipyc Nanoporous Metal Terephthalates MIL-53 and MIL-47. *J. Am. Chem. Soc.* **2005**, *127*, 13519–13521.

(34) Caskey, S. R.; Wong-Foy, A. G.; Matzger, A. J. Dramatic Tuning of Carbon Dioxide Uptake via Metal Substitution in a Coordination Polymer with Cylindrical Pores. *J. Am. Chem. Soc.* **2008**, *130*, 10870–10871.

(35) Yang, S.; Sun, J.; Ramirez-Cuesta, A. J.; Callear, S. K.; David, W. I. F.; Anderson, D. P.; Newby, R.; Blake, A. J.; Parker, J. E.; Tang, C. C.; Schröder, M. Selectivity and direct visualization of carbon dioxide and sulfur dioxide in a decorated porous host. *Nat. Chem.* **2012**, *4*, 887–894.

(36) Lee, S.; Kapustin, E.; Yaghi, O. M. Coordinative alignment of molecules in chiral metal-organic frameworks. *Science* **2016**, *353*, 808–811.

(37) Mon, M.; Ferrando-Soria, J.; Verdaguer, M.; Train, C.; Paillard, C.; Dkhil, B.; Versace, C.; Bruno, R.; Armentano, D.; Pardo, E. Postsynthetic Approach for the Rational Design of Chiral Ferroelectric Metal-Organic Frameworks. *J. Am. Chem. Soc.* **2017**, *139*, 8098–8101.

(38) Liu, Y.; Xi, X.; Ye, C.; Gong, T.; Yang, Z.; Cui, Y. Chiral Metal-Organic Frameworks Bearing Free Carboxylic Acids for Organocatalyst Encapsulation. *Angew. Chem., Int. Ed.* **2014**, *53*, 13821–13825.

(39) Zhang, S.-Y.; Li, D.; Guo, D.; Zhang, H.; Shi, W.; Cheng, P.; Wojtas, L.; Zaworotko, M. J. Synthesis of a Chiral Crystal Form of MOF-5, CMOF-5, by Chiral Induction. *J. Am. Chem. Soc.* **2015**, *137*, 15406–15409.

(40) Ferguson, A.; Liu, L.; Tapperwijn, S. J.; Perl, D.; Coudert, F.-X.; Van Cleuvenbergen, S.; Verbiest, T.; van der Veen, M. A.; Telfer, S. G. Controlled partial interpenetration in metal-organic frameworks. *Nat. Chem.* **2016**, 1–8.

(41) Grancha, T.; Ferrando-Soria, J.; Cano, J.; Amorós, P.; Seoane, B.; Gascon, J.; Bazaga-García, M.; Losilla, E. R.; Cabeza, A.; Armentano, D.; Pardo, E. Insights into the Dynamics of Grotthuss Mechanism in a Proton-Conducting Chiral *bio*MOF. *Chem. Mater.* **2016**, *28*, 4608–4615.

(42) Rosi, N. L.; Kim, J.; Eddaoudi, M.; Chen, B.; O'Keeffe, M.; Yaghi, O. M. Rod Packings and Metal-Organic Frameworks Constructed from Rod-Shaped Secondary Building Units. *J. Am. Chem. Soc.* **2005**, *127*, 1504–1518.

(43) Catarineu, N. R.; Schoedel, A.; Urban, P.; Morla, M. B.; Trickett, C. A.; Yaghi, O. M. Two Principles of Reticular Chemistry Uncovered in a Metal-Organic Framework of Heterotritopic Linkers and Infinite Secondary Building Units. *J. Am. Chem. Soc.* **2016**, *138*, 10826–10829.

(44) Grancha, T.; Qu, X.; Julve, M.; Ferrando-Soria, J.; Armentano, D.; Pardo, E. Rational Synthesis of Chiral Metal-Organic Frameworks from Preformed Rodlike Secondary Builidng Units. *Inorg. Chem.* **2017**, *56*, 6551–6557.

(45) (a) Wang, F.; Liu, Z.-S.; Yang, H.; Tan, Y.–X.; Zhang, J. Hybrid Zeolitic Imidazolate Frameworks with Catalytically Active TO4 Building Blocks. *Angew. Chem. Int. Ed.* **2011**, *50*, 450 –453. (b) Tang, Y.-H.; Wang F.; Liu, J.-X.; Zhang, J. Diverse tetrahedral tetrazolate frameworks with N-rich surface. *Chem. Commun.* **2016**, *52*, 5625–5628. (c) Liu, J.; Wang, F.; Liu, L.-Y.; Zhang, J. Interpenetrated Three-Dimensional Copper-Iodine Cluster-Based Framework with Enantiopure Porphyrin-like Templates. *Inorg. Chem.* **2016**, *55*, 1358–1360. (d) Liu, J.; Wang, F.; Zhang, J. Synthesis of Homochiral Zeolitic Tetrazolate Frameworks Based on Enantiopure Porphyrin-like Subunits. *Cryst. Growth Des.* **2017**, *17*, 5393–5397. (e) Tan, Y. X.; Wang, F.; Zhang, J. Design and synthesis of multifunctional metal-organic zeolites. *Chem. Soc. Rev.* **2018**, *47*, 2130–2144.

(46) (a) Grancha, T.; Mon, M.; Ferrando-Soria, J.; Armentano, D.; Pardo, E. Structural Studies on a New Family of Chiral BioMOFs. *Cryst. Growth Des.* **2016**, *16*, 5571–5578. (b) Grancha, T.; Mon, M.; Ferrando-Soria, J.; Gascon, J.; Seoane, B.; Ramos-Fernandez, E. V.; Armentano, D.; Pardo, E. Tuning the selectivity of light hydrocarbons in natural gas in a family of isoreticular MOFs. *J. Mater. Chem. A* **2017**, *5*, 11032–11039. (c) Mon, M.; X.; Ferrando-Soria, J.; Pellicer-Carreño, I.; Sepúlveda-Escribano, A.; Ramos-Fernandez, E. V.; Jansen, J. C.; Armentano, D.; Pardo, E. Fine-tuning of the confined space in microporous metal-organic frameworks for efficient mercury removal. *J. Mater. Chem. A* **2017**, *5*, 20120–20125.

(47) (a) Suh, M. P.; Moon, H. R. Coordination Polymer Open Frameworks Constructed of Macrocyclic Complexes. *Adv. Inorg. Chem.* **2006**, *59*, 39–79. (b) Zhu, J.; Usov, P. M.; Xu, W.; Celis-Salazar, P. J.; Lin, S.; Kessinger, M. C.; Landaverde-Alvarado, C.; Cai, M.; May, A. M.; Slebodnick, C.; Zhu, D.; Senanayake, S. D.; Morris, A. J. A New Class of Metal-Cyclam-Based Zirconium Metal-Organic Frameworks for CO_2 Adsorption and Chemical Fixation. *J. Am. Chem. Soc.* **2018**, *140*, 993–1003.

(48) (a) Lehn, J. M. Perspectives in Chemistry–Steps towards Complex Matter. *Angew. Chemie - Int. Ed.* **2013**, *52*, 2836–2850. (b) Lehn, J. M. Perspectives in Chemistry–Aspects of Adaptive Chemistry and Materials. *Angew. Chemie - Int. Ed.* **2015**, *54*, 3276–3289. (c) Ayme, J.-F.; Lehn, J.-M. From Coordination Chemistry to Adaptive Chemistry. *Advances in Inorganic Chemistry* **2018**, *71*, 3–78.

(49) Grancha, T.; Ferrando-Soria, J.; Cano, J.; Lloret, F.; Julve, M.; De Munno, G.; Armentano, D.; Pardo, E. Enantioselective self-assembly of antiferromagnetic hexacopper(II) wheels with chiral amino acid oxamates. *Chem. Commun.* **2013**, *49*, 5942–5944.

(50) Blatov, V. A. A method for topological analysis of rod packings. *Struct. Chem.* **2016**, *27*, 1605–1611.

(51) O'Keeffe, M.; Peskov, M. A.; Ramsden, S. J.; Yaghi, O. M. The Reticular Chemistry Structure Resource (RCSR) Database of, and Symbols for, Crystal Nets. *Acc. Chem. Res.* **2008**, *41*, 1782-1789.

(52) Blatov, V. A.; Shevchenko, A. P.; Proserpio, D. M. Applied Topological Analysis of Crystal Structures with the Program Package ToposPro. *Cryst. Growth Des.* **2014**, *14*, 3576–3586.

(53) Bonneau, C.; O'Keeffe, M.; Proserpio, D. M.; Blatov, V. A.; Batten, S. R.; Bourne, S. A.; Lah, M. S.; Eon, J.-G.; Hyde, S. T.; Wiggin, S. B.; Öhrström, L. Deconstruction of Crystalline Networks into Underlying Nets: Relevance for Terminology Guidelines and Crystallographic Databases. *Cryst. Growth Des.* **2018**, *18*, 3411-3418.

(54) see http://www.toris.com (accessed September 3 rd, 2018).

(55) Barthel, S.; Alexandrov, E. V.; Proserpio, D. M.; Smit, B. Distinguishing Metal–Organic Frameworks. *Cryst. Growth Des.* **2018**, *18*, 1738-1747.

(56) (a) Schreiner, P. R.; Chernish, L. V.; Gunchenko, P. A.; Tikhonchuk, E. Y.; Hausmann, H.; Serafin, M.; Schlecht, S.; Dahl, J. E. P.; Carlson, R. M. K.; Fokin, A. A. Overcoming lability of extremely long alkane carbon-carbon bonds through dispersion forces. *Nature* **2011**, 477, 308–311. (b) Echeverría, J.; Aullon, G.; Danovich, D.; Shaik, S.; Alvarez, S. Dihydrogen contacts in alkanes are subtle but not faint. *Nat. Chem.* **2011**, 3, 323–330. (c) Fokin, A. A.; Chernish, L. V.; Gunchenko, P. A.; Tikhonchuk, E. Y.; Hausmann, H.; Serafin, M.; Dahl, J. E.; Carlson, R. M. K.; Schreiner, P. R. Stable Alkanes Containing Very Long Carbon-Carbon Bonds. *J. Am. Chem. Soc.* **2012**, 134, 13641–13650.

(57) Ridgway, N; McLeod, R. Eds. *Biochemistry of Lipids, Lipoproteins and Membranes* (Elsevier, Amsterdam, 2015).

We report on the application of the metalloligand design strategy towards the development of efficient routes to obtain chiral rodlike MOFs. The as-made homochiral rodlike MOF (**2**) exhibits rare **etd** topology.